

Bent Molecules with a 60° Central Core Angle that Form B7 and B2 Phases**

Eun-Woo Lee, Koji Takimoto, Masatoshi Tokita, Junji Watanabe, and Sungmin Kang*

Abstract: Small-angle bent-core liquid-crystalline (LC) molecules based on a 1,2-bis(phenylethynyl)benzene central core have been synthesized that form banana smectic phases with a ferroelectric B7–antiferroelectric B2 phase sequence upon cooling. The formation of polar, switchable ferro-/antiferroelectric banana phases indicates that, despite the low core bend angle of approximately 60°, banana smectic phases are still formed with the bend direction parallel to the layer. This study offers significant evidence that shows bent-core molecules with a 60° bend angle can form the well-known B2 and B7 banana phases. Consequently, it may lead to the preparation of a wide variety of novel bent molecules with low bend angles that spontaneously form an LC phase with both polarization and chirality.

Banana-shaped LC molecules, or so-called bent-shaped or bent-core LC molecules, have fascinated a great number of researchers in the field of liquid crystal science since the initial report of their existence by Watanabe et al.^[1] Banana-shaped LCs have attracted much attention because of their distinct mesomorphic behavior, that is, the spontaneous formation of chirality and polarity from achiral molecules, which consequently induces a variety of smectic (Sm) sub-phases comprised of B1–B7 banana phases.^[2] Since the discovery of banana-shaped LC molecules,^[1] it has been thought that a bend angle of approximately 120° is appropriate for the formation of banana phases. Typical bent-core groups used for banana-shaped LC molecules include 1,3-disubstituted benzenes, 2,6-disubstituted pyridines, 2,7-disubstituted naphthalenes, and 3,4'-disubstituted biphenyls. The angles reported to date for these compounds, which form banana phases, range from 110° to 140°.^[3]

We have focused on smaller bend-angle molecules, and we are interested in determining the smallest critical bend angle at which polar packing of bent molecules occurs in the smectic layer. Early reports based on 1,2-phenylene and 2,3-naphthalene central cores with very small bend angles of approx-

imately 60° showed that only conventional nematic and smectic phases were formed.^[4] These molecules are assumed to have U-shaped conformations for which bent direction packing along the layer may not take place; therefore, they behave in a manner similar to that of conventional calamitic molecules, aligning their bent directions up and down in the layer.^[5] However, by synthesizing six different types of bent-shaped molecules with typical Schiff-base side wings on the various branching positions of the central naphthalene core,^[6] we have discovered that molecules composed of 1,7-naphthalene derivatives form typical banana phases, such as B4 and antiferroelectric smectic A (SmAP_A) phases, despite their small bend angles of approximately 60°. Also, for the same homologous series based on a 2,3-naphthalene central core, Ros et al. and Choi et al. reported different investigation results in which Choi et al. claimed a polar SmA phase,^[7] whereas Ros et al. interpreted it to be a non-polar SmA phase.^[8] Therefore, to observe not only polarity but also a direction of molecular director is still controversial. Furthermore, similar homologues based on a small-bend-angle 1,7-naphthalene core were found to form both a switchable hexagonal columnar (Col_h)^[9] and cubic (Cub) phases^[10] that are constructed of enclosed smectic layers. It is thus believed that the proper selection of central cores with a small bend angle can induce the promotion of not only bend direction molecular packing, which gives rise to the formation of polar banana phases, but also the formation of a diverse array of deformed layering structures, such as Col_h and Cub phases.

Herein, novel low-angle bent-core LC molecules based on a 1,2-bis(phenylethynyl)benzene central core, P(1,2)-On, containing seven aromatic rings and alkoxy tails with carbon numbers of 12, 16, and 18 (Scheme 1) were synthesized. This *ortho*-bistolane central core offers a 60° bend angle without conformational freedom.

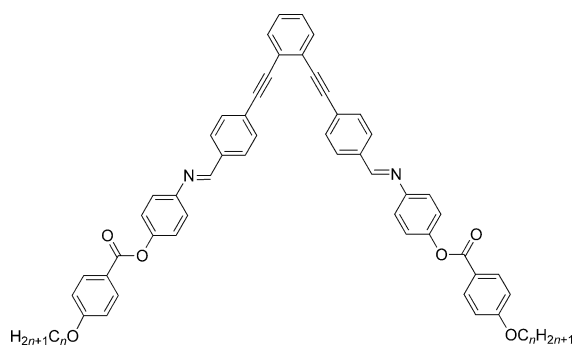
Figure 1 shows a representative differential scanning calorimetry (DSC) thermogram of P(1,2)-O18 upon heating and cooling at a scanning rate of 10°C min⁻¹. As observed in cooling DSC data, two endothermic peaks at 249 and 232°C were detected before crystallization at $T_c = 123^\circ\text{C}$ that correspond to the isotropic (Iso)–X and X–B7 phase transitions, respectively. Furthermore, a small peak due to the B7–B2 phase transition was observed at 159°C, as shown in the inset at enlarged scale (scanning rate: 10°C min⁻¹).

Figure 1 also presents the polarized optical microscopy (POM) images for each LC phase observed during the cooling process. The highest temperature of the X phase shows no birefringent texture at all; however, it is distinguished from the isotropic melt by a drastic fall in the fluidity at the Iso–X phase transition. Upon cooling of the X phase into the B7

[*] E.-W. Lee, K. Takimoto, Prof. Dr. M. Tokita, Prof. Dr. J. Watanabe, Prof. Dr. S. Kang
Organic and Polymeric Materials
Tokyo Institute of Technology
2-12-1 O-okayama, Tokyo 152-8552 (Japan)
E-mail: skang@polymer.titech.ac.jp

[**] This research was supported by a Grant-in-Aid for Scientific Research (c) (26410086) from the Ministry of Education, Culture, Sports, Science and Technology in Japan. The synchrotron radiation X-ray measurement was performed at the 4C beamline in the Pohang Light Source II (PLS-II).

Supporting information for this article is available on the WWW under <http://dx.doi.org/10.1002/anie.201403762>.



Scheme 1. Chemical structure of P(1,2)-On.

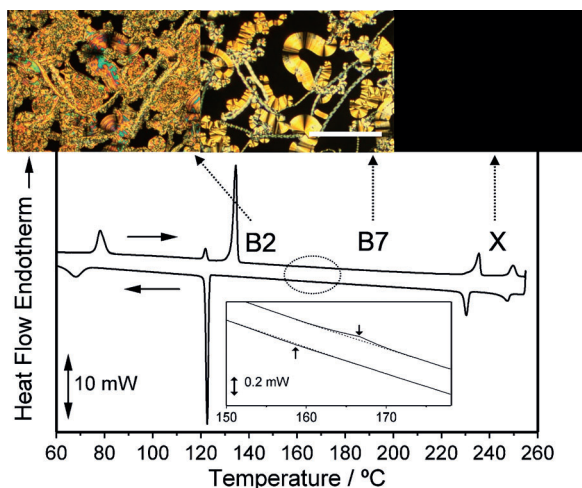


Figure 1. Typical DSC thermogram for P(1,2)-O18 with a scanning rate of $10^{\circ}\text{C min}^{-1}$. The inset shows enlarged peaks corresponding to the B7–B2 phase transition. POM observation images were taken at 234 °C, 220 °C, and 147 °C for the X, B7, and B2 phases, respectively, upon cooling. The B7 image was taken with a slow-cooling sample preparation ($1^{\circ}\text{C min}^{-1}$). Scale bar: 100 μm .

phase, typical myelinic helical filaments and a striped focal conical texture could be observed that are reminiscent of the B7 phase. Upon further cooling to the B2 phase, the overall shape of the texture was not significantly changed, although the birefringence increased and typical fringed and grainy textures were superimposed. Such a slight texture change between the B2 and B7 phases was expected given the very small peak in the aforementioned DSC thermogram.

The thermodynamic data and phase sequence information for P(1,2)-On obtained by the DSC and POM analyses are listed in Table 1 and Figure 2, respectively. At a glance, it can be seen that the effect of the terminal chain length, n , on the

Table 1: Phase-transition behaviors of P(1,2)-On upon cooling process with a scanning rate of $10^{\circ}\text{C min}^{-1}$.

Compound	Transition property [Temperature (Enthalpy): $^{\circ}\text{C}$ (kJ mol $^{-1}$)]
P(1,2)-O12	Cr 141 (27.1) B2 213 (0.4) B7 234 (14.4) Iso
P(1,2)-O16	Cr 124 (38.2) B2 174 (0.2) B7 232 (10.5) X 245 (2.7) Iso
P(1,2)-O18	Cr 123 (49.8) B2 159 (0.2) B7 230 (12.4) X 247 (5.8) Iso

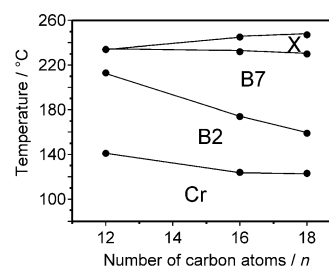


Figure 2. Phase-transition behaviors of P(1,2)-On determined by DSC measurements with a scanning rate of $10^{\circ}\text{C min}^{-1}$.

phase sequential properties is significant. As n decreased from 18 to 16, the phase-transition sequence was unchanged, but the B7 LC regime became narrower owing to an elevation of the B7–B2 transition temperature. A further decrease in n to 12 led to the disappearance of the X phase and the appearance of the B7 phase directly from the isotropic melt followed by the B2 LC regime.

Of most interest is the formation of the B2 and B7 phases. Electro-optical measurements clarified the polar switching nature of the B7 and B2 phases. Typical textural transformations were observed in the initial circular domain for $n = 18$ by applying a voltage, as shown in Figure 3. Without the applied field, the extinction brush was lying parallel to the cross-nicol direction. When either a plus or minus DC voltage was applied, the birefringence increased slightly, but the extinction direction remained unchanged. Additionally, when the triangular wave field was reversed, a single reversal current peak was observed within a half period of the triangular wave voltage (Figure 3b). This switching behavior can be explained by the presence of an anticlinic ferroelectric layer structure; in other words, a SmC_AP_F layer structure (Figure 3c).

On the other hand, the B2 phase exhibited a grainy circular domain when observed at the same position. Upon application of a field, it immediately transformed into a clear circular domain with the extinction direction parallel to the cross-nicol direction, as seen under field. Additionally, when a triangular wave voltage was applied, two reversal peaks were observed within a half period (Figure 4b). Thus, the ground state of the layer structure for B2 can be explained by a synclitic antiferroelectric SmC_SP_A structure (See Figure 4c). The spontaneous polarization (P_s) value calculated by integrating the reversal current peaks was fairly large (ca. 800 nC cm^{-2}) for the B2 phase, while for the P_s value for the B7 phase was less than 200 nC cm^{-2} (Supporting Information, Figure S1). Furthermore, the second harmonic generation (SHG) was measured for the two phases during application of the field. The SH signals showed the same tendency as the P_s values, increasing upon the B7–B2 phase transition. Based on the previously observed switching behavior of these types of compounds, the B7 phase has been divided into subgroups according to its switching ability, that is, non-switchable B7 and switchable B7' phases.^[11,2g] In the present case, therefore, the B7 phase should be classified as a B7' phase.

Next, an X-ray analysis was carried out to clarify the structure in more detail using both wide-angle X-ray diffrac-

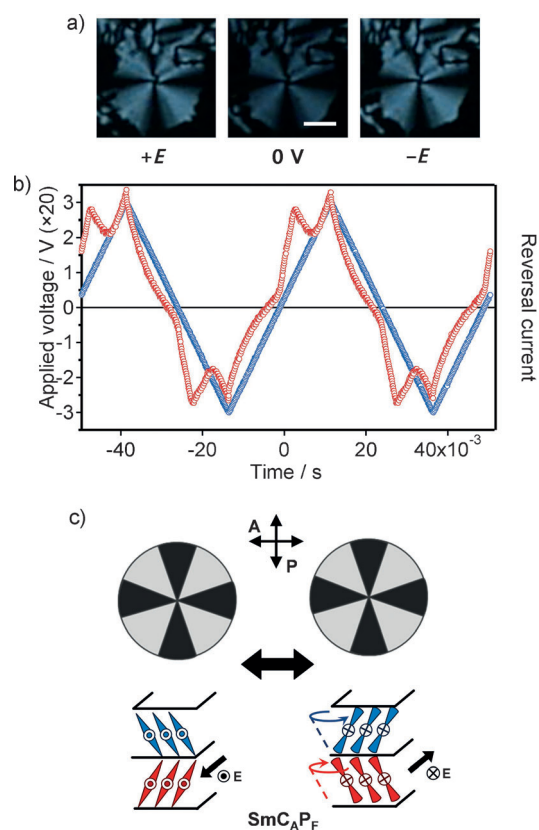


Figure 3. Electro-optic properties of B7 phase for P(1,2)-O18 measured at 200 °C. a) POM observations during the application of DC voltage (cell gap: 1.8 μm , DC: 60 V), b) polarization reversal current (cell gap: 1.9 μm , 120V_{pp}), and c) an illustration of the polar layer structure of the B7 phase. Scale bar: 10 μm .

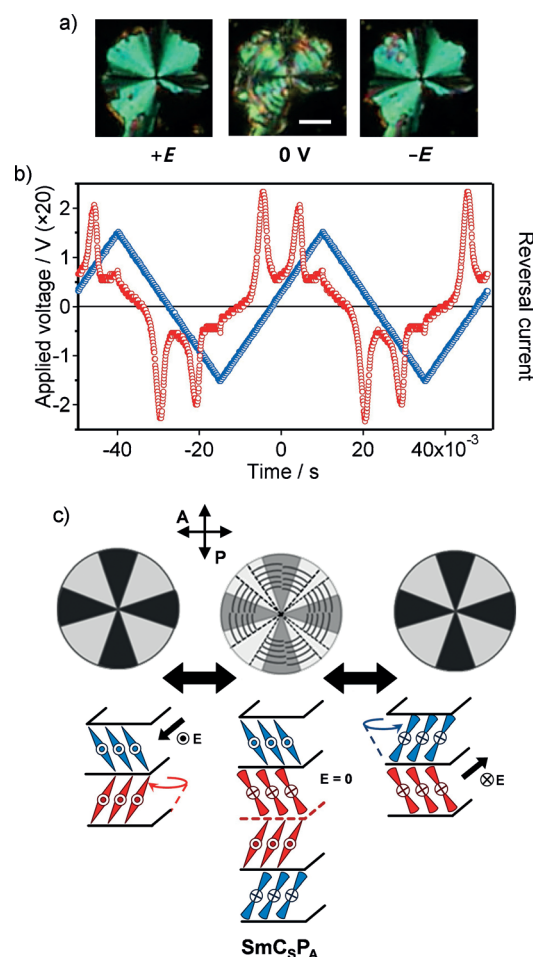


Figure 4. Electro-optic properties of B2 phase for P(1,2)-O18 measured at 145 °C. a) POM observations during the application of DC voltage (cell gap: 1.8 μm , DC: 40 V), b) polarization reversal current (cell gap: 1.9 μm , 120V_{pp}), and c) an illustration of the polar layer structure of the B2 phase. Scale bar: 10 μm . The layer structure of ground state contains two different domains (the dotted line indicates the domain boundary).

tion (WAXD) and small-angle X-ray scattering (SAXS) (Supporting Information, Table S1). Figure 5a shows the one-dimensional (1D) and two-dimensional (2D) SAXS profiles for P(1,2)-O18 during cooling. Upon entering the X phase at 250 °C, a broad reflection at $q (= 2\pi/d) = 2\pi/88.3 \text{ \AA}^{-1}$ (where d indicates d -spacing) appeared; therefore, the optically isotropic X phase could be distinguished again from the isotropic melt (see also the 2D patterns). Upon further cooling to the B7 phase at 220 °C, a set of multiscattering peaks appeared in the small angle region that were incommensurate. The strongest diffraction at $2\pi/46.5 \text{ \AA}^{-1}$ seemed to stem from the layering order of the B7 phase. Eventually, the inner angled multiple reflections disappeared along with a slight simultaneous change in the d -spacing of the layer reflection at $2\pi/47.5 \text{ \AA}^{-1}$ upon formation of the B2 phase. It should also be noted that during the consecutive phase transitions of the X–B7–B2 phases, the diffuse wide angle diffractions at $2\pi/4.4 \text{ \AA}^{-1}$ in each LC phase were observed in the WAXD patterns (Figure 5b), indicating a liquid-like lateral packing of molecule in each LC phase. Moreover, the tilt angle in the B2 phase was estimated as 36.2° for $n=18$ based on the most extended chain model obtained by a Spartan 10 calculation (Supporting Information, Table S2 and Figure S2).

Finally, the B7 phase was extensively examined using a homeotropically aligned sample and synchrotron-radiation SAXS measurement. Figure 6 presents the oriented SAXS profile collected at 220 °C. Along the meridional line, a pair of the strongest layer reflections with a spacing of 46.5 \AA was concentrated, indicating that smectic layering also developed along this line direction. However, the inner satellite reflections with spacings of 55.2, 76.2, 110.4, and 157.7 \AA show split patterns from this line with different split angles. These observations suggest a frustrated structure with a two-dimensional oblique lattice in which $a = 401 \text{ \AA}$, $c = 170 \text{ \AA}$, and $\beta = 16^\circ$, similar to the previously reported 2D oblique lattice, which is composed of layer blocks with same slope in the B7 phase.^[12] Thus, the (100) reflection of (h00) and only (101), (201) reflections of (h01) showed enough intensity to be observed.^[12b] Additionally, the value of the lattice parameter a depended on the temperature, increasing from 400 to 600 \AA as the temperature decreased from 220 to 195 °C. Thus, it can be concluded that the B7 phase can be attributed to a well-

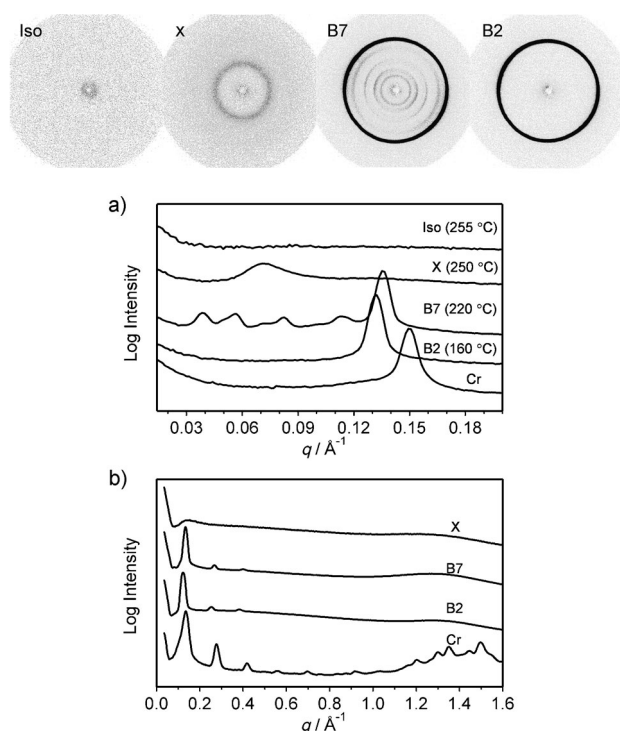


Figure 5. 1D and 2D profiles of X-ray investigations of powder sample for P(1,2)-O18. One-dimensional a) SAXS and b) WAXD profiles obtained from each phase. In the upper row, 2D SAXS patterns measured at Iso (255 °C), X (250 °C), B7 (220 °C), and B2 (160 °C) phases are shown.

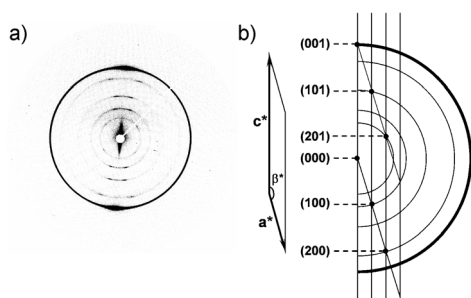


Figure 6. a) 2D oriented SAXS profiles at 220 °C for P(1,2)-O18 and b) a reciprocal lattice structure interpreted as a 2D oblique lattice ($a = 401 \text{ \AA}$, $c = 170 \text{ \AA}$, and $\beta = 16^\circ$). Here, every diffraction spot matched well with the indexation of $(h0l)$.

known frustrated structure in which layer undulation and/or polarization modulation have occurred resulting in the formation of an oblique 2D lattice (as proposed in Figure 7). It is believed that the increase in the birefringence upon application of a voltage may be understood as the rearrangement of the polarization splay deformation in the B7 phase.

In conclusion, this study revealed the formation of typical banana phases of B7 and B2 in a novel bent-core system with a significantly small bend angle of 60° . Despite the low bend angle, the formation of the polar switchable ferro-/antiferro-electric banana phases is indicative of smectic layering by

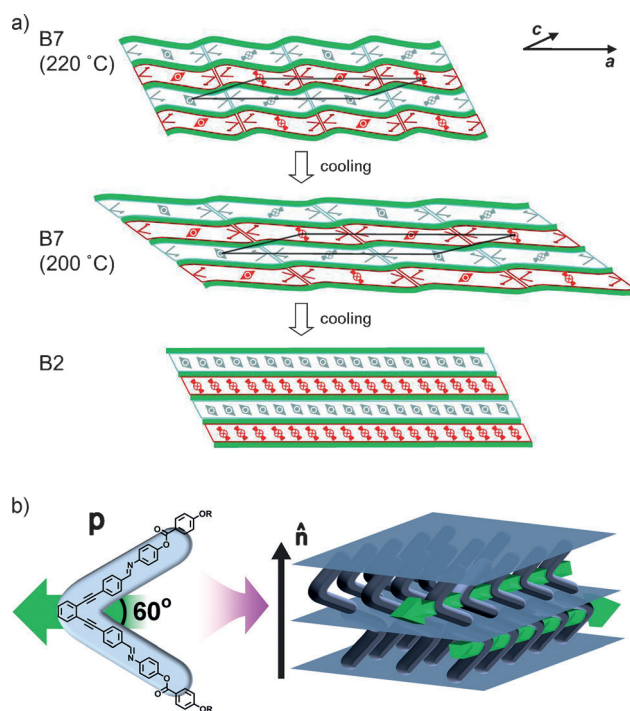


Figure 7. a) Illustration of possible structural transformation occurring at the B7–B2 phase transition and real lattice structure of the B7 phase. Here, the polarization splay modulation takes place, forming a frustration explained by a 2D oblique lattice. b) Three-dimensional representation of the B2 phase structure in which a molecular packing in a bent direction along the layer is established; in other words, the direction of n -director lies in the layer normal.

molecular packing along the molecular bend direction. This result is striking because it had been believed that banana phases can only be stabilized when the bending angle is in the range from 110 – 140° , and these results thus provide additional insight into the nature of banana-shaped molecules. Further investigation of the relationship between the ultimate molecular shape and the formation of banana LCs is, however, still needed.

Received: March 27, 2014

Published online: June 24, 2014

Keywords: banana phases · bent-shaped molecules · ferro/antiferro-electricity · liquid crystals · X-ray diffraction

[1] T. Niori, T. Sekine, J. Watanabe, T. Furukawa, H. Takezoe, *J. Mater. Chem.* **1996**, *6*, 1231–1233.

[2] a) D. R. Link, G. Natale, R. Shao, J. E. MacLennan, N. A. Clark, E. Körblova, D. M. Walba, *Science* **1997**, *278*, 1924–1927; b) J. Watanabe, T. Niori, T. Sekine, H. Takezoe, *Jpn. J. Appl. Phys. Part 2* **1998**, *37*, L139–L142; c) G. Pelzl, S. Diele, W. Weissflog, *Adv. Mater.* **1999**, *11*, 707–724; d) J. Thisayukta, H. Takezoe, J. Watanabe, *Jpn. J. Appl. Phys.* **2001**, *40*, 3277–3287; e) D. A. Coleman, J. Fernsler, N. Chattham, M. Nakata, Y. Takaniishi, E. Körblova, D. R. Link, R.-F. Shao, W. G. Jang, J. E. MacLennan, O. Mondainn-Monval, C. Boyer, W. Weissflog, G. Pelzl, L. C. Chien, J. Zasadzinski, J. Watanabe, D. M. Walba, H. Takezoe, N. A. Clark, *Science* **2003**, *301*, 1204–1211; f) Y. Takaniishi, H.

- Takezoe, *Jpn. J. Appl. Phys.* **2006**, *45*, 597–625; g) R. A. Reddy, C. Tschierske, *J. Mater. Chem.* **2006**, *16*, 907–961.
- [3] a) I. Wirth, S. Diele, A. Eremin, G. Pelzl, S. Grande, L. Kovalenko, N. Pancenko, W. Weissflog, *J. Mater. Chem.* **2001**, *11*, 1642–1650; b) S. Kang, Y. Saito, N. Watanabe, M. Tokita, Y. Takanishi, H. Takezoe, J. Watanabe, *J. Phys. Chem. B* **2006**, *110*, 5205–5214.
- [4] a) H. Matsuzaki, Y. Matsunaga, *Liq. Cryst.* **1993**, *14*, 105–120; b) M. Kuboshita, Y. Matsunaga, H. Matsuzaki, *Mol. Cryst. Liq. Cryst.* **1991**, *199*, 319–326; c) C. V. Yelamaggad, I. Shashikala, D. S. S. Rao, S. K. Prasad, *Liq. Cryst.* **2004**, *31*, 1027–1036.
- [5] Y. Naito, R. Ishige, M. Itoh, M. Tokita, J. Watanabe, *Chem. Lett.* **2008**, *37*, 880–881.
- [6] a) S. K. Lee, Y. Naito, L. Shi, M. Tokita, H. Takezoe, J. Watanabe, *Liq. Cryst.* **2007**, *34*, 935–943; b) S. K. Lee, M. Tokita, H. Takezoe, J. Watanabe, *Ferroelectrics* **2008**, *365*, 1–11; c) S. K. Lee, L. Shi, R. Ishige, S. Kang, M. Tokita, J. Watanabe, *Chem. Lett.* **2008**, *37*, 1230–1231; d) S. K. Lee, X. Li, S. Kang, M. Tokita, J. Watanabe, *J. Mater. Chem.* **2009**, *19*, 4517–4522.
- [7] a) E.-J. Choi, X. Cui, C.-W. Ohk, W.-C. Zin, J.-H. Lee, T.-K. Kim, *J. Mater. Chem.* **2010**, *20*, 3743–3749; b) E.-J. Choi, E.-C. Kim, S.-B. Park, W.-C. Zin, Y.-J. Lee, J.-H. Kim, *J. Mater. Chem.* **2012**, *22*, 24930–24935.
- [8] a) N. Gimeno, M. J. Clemente, P. Forcén, J. L. Serrano, M. B. Ros, *New J. Chem.* **2009**, *33*, 2007–2014; b) I. Alonso, J. Martinez-Perdiguero, J. Ortega, C. L. Folcia, J. Etxebarria, N. Gimeno, M. B. Ros, *Liq. Cryst.* **2010**, *37*, 1465–1470.
- [9] a) X. Li, S. Kang, S. K. Lee, M. Tokita, J. Watanabe, *Jpn. J. Appl. Phys.* **2010**, *49*, 121701; b) X. Li, M. Zhan, K. Wang, *New J. Chem.* **2012**, *36*, 1133–1136.
- [10] S. Kang, M. Harada, X. Li, M. Tokita, J. Watanabe, *Soft Matter* **2012**, *8*, 1916–1922.
- [11] a) G. Pelzl, S. Diele, A. Jakli, W. Weissflog, *Liq. Cryst.* **2006**, *33*, 1513–1518; b) C. L. Folcia, J. Etxebarria, J. Ortega, M. B. Ros, *Phys. Rev. E* **2005**, *72*, 041709.
- [12] a) N. Vaupotič, M. Čopič, E. Gorecka, D. Pocięcha, *Phys. Rev. Lett.* **2007**, *98*, 247802; b) D. A. Coleman, C. D. Jones, M. Nakata, N. A. Clark, D. M. Walba, W. Weissflog, K. Fodor-Csorba, J. Watanabe, V. Novotna, V. Hamplova, *Phys. Rev. E* **2008**, *77*, 021703.